Clinical Chemistry 51:10
1962–1972 (2005)

Oak Ridge Conference

Direct Quantification of Analyte Concentration by Resonant Acoustic Profiling

Benjamin Godber, Kevin S.J. Thompson, Marian Rehak, Yildiz Uludag, Sven Kelling, Alexander Sleptsov, Mark Frogley, Klaus Wiehler, Christopher Whalen, and Matthew A. Cooper*

Background: **Acoustic sensors that exploit resonating quartz crystals directly detect the binding of an analyte to a receptor. Applications include detection of bacteria, viruses, and oligonucleotides and measurement of myoglobin, interleukin 1β (IL-1β), and enzyme cofactors.**
Methods: **Resonant Acoustic Profiling™ was combined with a microfluidic lateral flow device incorporating an internal reference control, stable linker chemistry, and immobilized receptors on a disposable sensor "chip". Analyte concentrations were determined by analyzing the rate of binding of the analyte to an appropriate receptor.**
Results: **The specificity and affinity of antibody–antigen and enzyme–cofactor interactions were determined without labeling of the receptor or the analyte. We measured protein concentrations (recombinant human IL-1β and recombinant human myoglobin) and quantified binding of cofactors ($NADP^+$ and NAD^+) to the enzyme glucose dehydrogenase. Lower limits of detection were ~1 nmol/L (17 ng/mL) for both IL-1β and human myoglobin. The equilibrium binding constant for $NADP^+$ binding to glucose dehydrogenase was 2.8 mmol/L.**
Conclusions: **Resonant Acoustic Profiling detects analytes in a relatively simple receptor-binding assay in <10 min. Potential applications include real-time immunoassays and biomarker detection. Combination of this technology platform with existing technologies for concentration and presentation of analytes may lead to simple, label-free, high-sensitivity methodologies for reagent and assay validation in clinical chemistry and, ultimately, for real-time in vitro diagnostics.**

Akubio Ltd., Cambridge, United Kingdom.
*Address correspondence to this author at: Akubio Ltd., Unit 181, Cambridge Science Park, Cambridge CB4 0GJ, UK. Fax 44-1223-225336; e-mail mcooper@akubio.com.
Received April 26, 2005; accepted July 18, 2005.
Previously published online at DOI: 10.1373/clinchem.2005.053249

Many polymers, ceramics, and molecules are polarized, and when an electric field is applied, the molecules will align themselves with it, producing induced dipoles within the molecular or crystal structure of the material. A permanently polarized material such as quartz (SiO_2) will produce an electric field when the material changes dimensions as a result of an imposed mechanical force. This material is termed piezoelectric, and the phenomenon is known as the piezoelectric effect *(1)*. This signal transduction mechanism, which forms the basis of acoustic sensing, was in fact first discovered by the Curie brothers in 1880 *(2)*. Today, acoustic sensors are generally based on quartz crystal resonators that are found in electronic devices such as watches, computers, and televisions, with more than 1 billion units mass-produced each year. Quartz crystal resonators became of interest to physicists and chemists when it was demonstrated that there is a linear relationship between mass adsorbed to the surface and the resonant frequency of the crystal in air or a vacuum *(3)*. Application to biological samples became possible when suitable oscillator circuits for operation in liquids were developed *(4, 5)*. As molecules interact with immobilized receptors on the surface of a quartz crystal, there is a concomitant modulation of the acoustic resonance of the crystal. This in turn produces a modulated electrical signal that can be analyzed by standard digital signal-processing techniques. The quartz crystal thus can be used as a very sensitive "microphone" to detect the presence of an analyte. The signal indicates not only the presence of the analyte but also the specificity and affinity for a surface-bound receptor.

By monitoring the change in resonance frequency and resistance that occurs on adsorption of an analyte to the surface (Fig. 1), quartz crystal resonators can be used to characterize interactions with small molecules *(6–8)*, peptides *(9–11)*, proteins and immunoassay markers *(12–18)*, oligonucleotides *(19, 20)*, bacteriophages *(21–23)*, viruses *(24–26)*, bacteria *(27–32)*, and cells *(33–41)*. The technology can thus be applied to an extremely wide range of

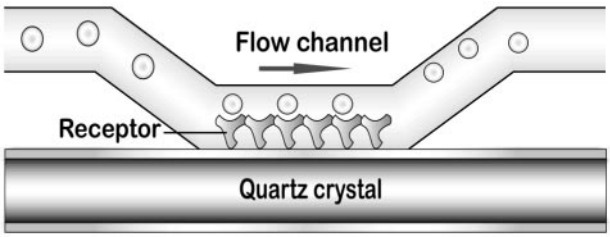

Fig. 1. Pictorial representation of a piezoelectric bioassay.

A piezoelectric acoustic wave device (such as a quartz crystal resonator) is coated with a selective, passivating layer on which an analyte-specific receptor can be immobilized. Liquid containing the analyte of interest is then passed across the surface by appropriate microfluidics, which enables selective capture of the analyte. This additional bound material in turn modulates resonance of the acoustic wave device, which is transformed into an electrical signal via the piezoelectric effect.

biological and chemical entities with a molecular weight range from M_r <200 through to an entire cell. Real-time monitoring of changes in the resonance properties of the crystal allows the label-free determination of interaction affinities and kinetics, as is the case for optical biosensors that exploit interfacial evanescence and/or surface polaritons *(42)*. However, acoustic sensors are more than just simple mass balances. Much more detailed information can be obtained about an interaction than is the case with optical biosensors because the acoustic sensor response is sensitive not only to the mass of analyte bound, but also to changes in the viscoelastic properties and charge of the receptor–analyte complex *(43, 44)*.

The majority of platforms currently used in clinical diagnosis require some type of radioactive, enzymatic, chemiluminescent, or fluorescent labeling to report the binding of an analyte to a receptor. This labeling step imposes additional time and cost demands, and can in some cases interfere with the molecular interaction by occluding a binding site, leading to false negatives/low sensitivity. Many reporter compounds are also hydrophobic, and in many screens, background binding is a major problem, leading to false positives/low specificity. We have developed a novel acoustic detection technology, that we term Resonant Acoustic Profiling™ (RAP™). This technology builds on the fundamental basics of the quartz crystal microbalance (QCM)[1] with several key additional features that are detailed in the *Materials and Methods* and *Results and Discussion* sections. This system generates high-quality, high–information-content data in real time, which can be analyzed to give quantitative information regarding analyte concentration as well as analyte–receptor interaction specificities, affinities, and kinetics. In this report we review published work from older QCM systems and highlight early progress made from application of RAP to selected clinically relevant molecular interactions.

Materials and Methods

INSTRUMENTATION AND SENSORS

RAP experiments were conducted with manually operated or automated prototype 2-channel instruments (Akubio Ltd). The automated instrument was based on a Tecan MSP9250 liquid-handling robot. The Akubio instruments apply the principles of QCM in that a high-frequency voltage is applied to a piezoelectric quartz crystal to induce the crystal to oscillate, and its resonance frequency is monitored in real time. The resonant frequencies of the sensors are determined by a proprietary network analyzer approach similar to that described elsewhere *(5, 45)*. In brief, to derive the resonant frequency and acoustic load parameters, the complex impedance of the resonator is acquired over a frequency range of ~50 kHz. These data are then subjected to a nonlinear fit against a modified Butterworth–VanDyke model of acoustic impedance *(46, 47)*.

The dual-channel sensors are composed of a pair of oscillating resonators mounted on a single quartz plate, which is sealed into parallel microfluidic flow cells fabricated by micromachining from acrylic. The assembled microfluidics cassette allows a sample to be flowed across 2 surfaces simultaneously, or individually, by use of separate flow paths to individual flow cells combined with a common flow path split to address both flow cells. Interchange between the different flow paths was by either manual or electronically operated valves (Akubio). As sample is flowed across "control" and "active" sensors, binding to the active sensor is measured as a reduction in the oscillation frequency, with the control sensor acting as a subtractive sample reference.

Sensors were constructed from standard quartz wafers (Roditi International) that are produced from bare quartz resonators coated by electron beam deposition with a titanium adhesion layer and a gold adlayer. These sensors were then further derivatized with a carboxylic acid-terminated interfacial layer deposited from ethanolic solution to provide a surface suitable for protein immobilization. The RAP instruments were fitted with a thermally stable sensor mounting block, which provided temperature control, and with microfluidic and electrical connections to the pair of piezoelectric resonators in the sensor cassette. Buffer flow was maintained with the Tecan robot syringe pumps (Tecan UK) under control of proprietary software (Akubio).

SENSOR SURFACE PREPARATION

For mouse IgG, myoglobin, and interleukin 1β (IL-1β) binding assays, before assessment of antigen binding, sensor surfaces were prepared. Briefly, rabbit anti-mouse Fc-specific immunoglobulin (RaM-Fc) and mouse IgG (Ms IgG) were immobilized on the active sensor surface and

[1] Nonstandard abbreviations: QCM, quartz crystal microbalance; IL-1β, interleukin 1β; RaM-FC, rabbit anti-mouse (Fc-specific) immunoglobulin; Ms IgG, mouse IgG; EDC, 1-ethyl-3-[3-dimethylaminopropyl]carbodiimide hydrochloride; NHS, *N*-hydroxysuccinimide; PBS, Dulbecco modified phosphate-buffered saline; GDH, glucose dehydrogenase (EC 1.1.1.47); BSA, bovine serum albumin; and GMO, genetically modified organism.

the control sensor surface, respectively, by conventional amine coupling chemistry. Sensor surfaces were activated with a 1:1 mixture of 400 mmol/L 1-ethyl-3-[3-dimethylaminopropyl]carbodiimide hydrochloride (EDC) and 100 mmol/L *N*-hydroxysuccinimide (NHS; both from Perbio Science UK), which were prepared separately in 0.22 μm–filtered deionized water and mixed immediately before use (final concentrations, 200 mmol/L EDC and 50 mmol/L NHS). The EDC-NHS mixture was injected simultaneously across both sensor surfaces for 3 min. Affinity-purified RaM-Fc (Stratech Scientific Ltd/Jackson ImmunoResearch) and Ms IgG (Stratech/Jackson) were prepared for immobilization at 50 mg/L in immobilization buffer (10 mmol/L sodium acetate, pH 4.5) and were injected simultaneously across separate sensor surfaces for 3 min. Nonreacted NHS esters were then capped with 1 mol/L ethanolamine (Sigma-Aldrich) prepared in 0.22 μm–filtered deionized water (pH 8.5). The running buffer between sample injections was Dulbecco's modified phosphate-buffered saline (PBS; Sigma-Aldrich) at a flow rate of 50 μL/min.

Ms IgG binding assay

Ms IgG was prepared at 10 mg/L in PBS and injected across both active and control sensor surfaces for 1 min. After a dissociation period of 3 min, sensor surfaces were regenerated with a 1-min injection of 100 mmol/L HCl followed by a 30-s injection of 20 mmol/L NaOH.

myoglobin binding assay

Mouse monoclonal anti-myoglobin (Spectral Diagnostics) was prepared at 5 mg/L in HEPES-buffered saline (10 mmol/L HEPES, 120 mmol/L NaCl, 3 mmol/L EDTA) containing 0.05 mL/L Tween 20 (Sigma-Aldrich), and was captured on the RaM-Fc surface by injection across both sensor surfaces for 3 min. A dissociation period of 5 min under HEPES-buffered saline flow allowed the capture and dissociation of anti-myoglobin to stabilize. Recombinant human myoglobin (Spectral Diagnostics) was prepared at 5 mg/L in HEPES-buffered saline and then diluted further in ~3-fold dilutions to 17 μg/L. Myoglobin samples were injected for 5 min, followed by a 5-min dissociation period. Sensor surfaces were then regenerated as for the Ms IgG binding assay. Myoglobin binding curves were superimposed and normalized to the start of the sample injection. Initial binding rates were calculated from a linear fit model applied to the initial portion of each binding curve. Initial binding rate slopes were plotted against myoglobin concentration to generate a concentration-response calibration curve. Myoglobin concentrations in unknown samples were quantified by interpolation from this calibration curve.

IL-1β binding assay

Mouse monoclonal anti-IL-1β (R&D Systems Europe) was prepared at 5 mg/L in PBS containing 0.05 mL/L Tween 20 and was captured on the RaM-Fc surface by injection across both sensor surfaces for 3 min. A dissociation period of 6 min under buffer flow allowed the capture and dissociation of anti-IL-1β to stabilize. Recombinant human IL-1β (R&D Systems) was prepared at 12 nmol/L in PBS containing 0.05 mL/L Tween 20, and then was diluted further in 2-fold dilutions to 0.75 nmol/L. IL-1β samples were injected for 5 min, followed by a 5-min dissociation period. Sensor surfaces were regenerated with a 30-s injection of 20 mmol/L NaOH.

glucose dehydrogenase substrate selectivity and affinity

Glucose dehydrogenase (GDH; Sigma-Aldrich) was supplied in Tris buffer, which is unsuitable for amine coupling. Consequently, a NAP5 column (GE Healthcare/Amersham Biosciences, Amersham) was preequilibrated with 10 mL of immobilization buffer [10 mmol/L sodium acetate (pH 4.5), 0.5 mol/L glucose; Sigma-Aldrich]. GDH was diluted to 100 mg/L in immobilization buffer, and 200 μL was added to the column. An additional 200 μL of immobilization buffer was added to the column, and the column allowed to equilibrate. GDH was eluted by adding 2 mL of immobilization buffer and collecting 2-drop (~100-μL) fractions. GDH activity, measured by a spectrophotometric GDH + glucose + $NADP^+$ turnover assay, was found to elute in fractions 5–9. Consequently, these fractions were pooled. The final GDH concentration was 22 mg/L in immobilization buffer, pH 4.5. Bovine serum albumin (BSA; Sigma-Aldrich), as a nonbinding control, was prepared at 50 mg/L in 10 mmol/L sodium acetate buffer (pH 4.5) without glucose.

Sensor surfaces were activated with EDC-NHS for 8 min. GDH or BSA was then injected simultaneously across separate sensor surfaces for 4 min. Nonreacted NHS esters were capped with 1 mol/L ethanolamine (pH 8.5) for 8 min. The running buffer between sample injections was PBS containing 0.05 mL/L Tween 20 at a flow rate of 50 μL/min.

$NADP^+$ (Sigma-Aldrich), NAD^+ (Sigma-Aldrich). and FAD (Sigma-Aldrich) as GDH-binding cofactors were prepared at 2 mmol/L in running buffer and diluted in 4 steps to 222 μmol/L. Cofactors at each concentration were injected across GDH active and BSA control surfaces for 1 min, allowed to dissociate for 1 min, and then were injected a second time. After a 2-min cleaning period in running buffer, the next cofactor concentration was tested in duplicate. To calculate the equilibrium binding constant (K_D) for $NADP^+$ binding to GDH, $NADP^+$ was prepared at 2 mmol/L in running buffer and diluted in 3-fold dilutions to 25 μmol/L. Each $NADP^+$ concentration was injected for 1 min and then allowed to dissociate for 1 min, in duplicate. Equilibrium binding was calculated for each $NADP^+$ concentration by taking the mean response amplitude over a 10-s interval during the plateau phase of binding. K_D was calculated by plotting $NADP^+$ concentration against mean equilibrium binding

response amplitude and fitting this to a sigmoidal single-site binding model.

Results and Discussion

LITERATURE TRENDS

There has been an explosion of growth in the number of publications reporting QCM used to probe biological and chemical interactions in life sciences research and, to a lesser extent, in clinical diagnostics. The number of publications involving the use of QCM has increased rapidly since the mid-1980s, in particular, since the 1990s (Fig. 2A). Many of the separate hardware components that make up an acoustic biosensor are commercially available from numerous electronics companies: a lock-in amplifier, a frequency synthesizer, a power supply, and a quartz-crystal holder. This provides a low barrier to entry for the academic or industrial researcher compared with the expense and expertise required to assemble an optical platform (which usually requires a sophisticated charge-coupled device camera, processing software, optical filters, optical interfaces, lasers, and other components). As a result, from 1990 to 2000 the number of publications involving QCM grew semiexponentially; the rate of growth slowed slightly from 2000 to 2004 (Fig. 2A).

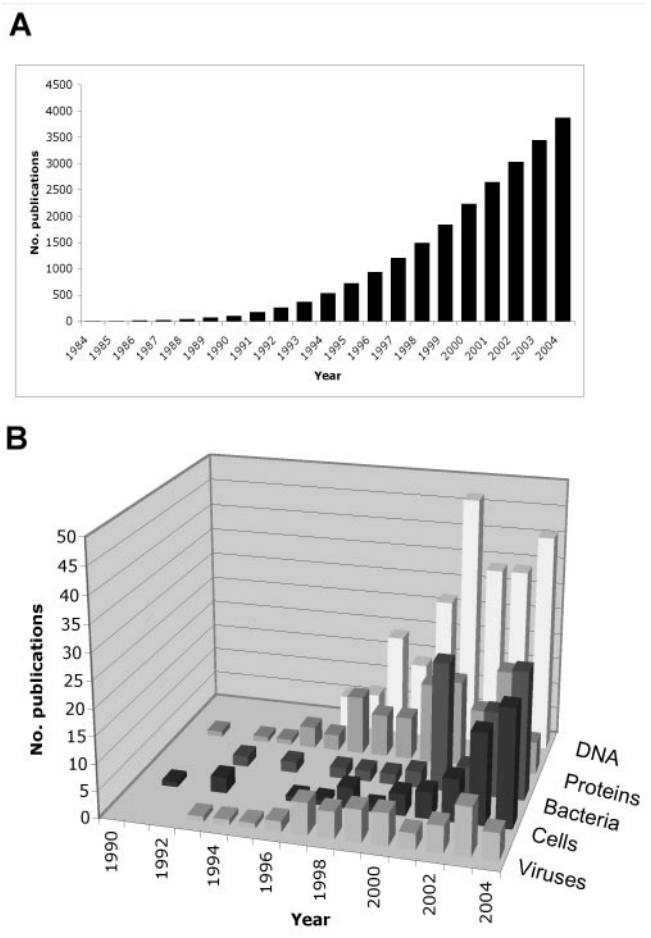

Fig. 2. Yearly cumulative number of publications citing use of QCM.

(*A*), publications found during an ISI Web of SCIENCE® search for the term "quartz crystal microbalance" in the title, keyword, or abstract. (*B*), publications found during an ISI Web of SCIENCE search for the term "quartz crystal microbalance" cross-referenced to the terms "DNA", "proteins OR immunoassay", "bacteria", "cell", or "virus".

This period has also seen an increase in the number of publications describing the detection and quantification of clinically relevant analytes *(12–18)* (Fig. 2B). Published limits of direct detection for analytes present in serum, blood, or urine are typically in the range of 0.1–10 mg/L (Table 1). Although these limits of detection can meet or surpass the clinically relevant limits of detection for many analytes, there are numerous other examples in which detection of nanogram per liter or even picogram per liter concentrations is required for accurate diagnosis. However, it is notable that these data were generated on "home-built" QCM systems, often with the use of very basic receptor attachment chemistries.

There has been a steady growth in the number of published reports describing detection of clinically relevant bacteria *(27–32)* (Fig. 2B), and in the last 5 years, there has been a rapid growth in the number of publications using acoustic biosensors to analyze mammalian cells *(33–41)*. In the latter application, a variety of cell types have been immobilized on quartz resonators coated with appropriate attachment chemistries. Here the cell forms an active part of the biological transducer component of the sensor, as bulk viscoelastic changes in the cell are also detected via the quartz resonator. This approach has been used to monitor interactions between cells and the adherent surface, as well as the cellular response to a variety of exogenous stimuli. Both the magnitude and kinetics of the response can be followed because detection occurs in real-time and does not require fluorescent, chemiluminescent, quantum dot, or other reporter labels.

The number of publications using acoustic sensing to

Table 1. Selected published data for acoustic detection of clinically relevant analytes using standard QCM instrumentation and a piezoelectric immunoassay.

Analyte	Matrix	Limit of detection	Reference
African swine fever virus	Serum	Ag:[a] 1 mg/L IgG: 0.2 mg/L	*(59)*
Anti-*Toxoplasma gondii* IgG	Blood, serum	1:5500 dilution	*(60)*
Anti-*Treponema pallidum* IgG	Serum	75 IU/L	*(61)*
Complement C4	Serum	0.1 mg/L	*(62)*
C-reactive protein	Serum	10 mg/L	*(12)*
Dermatophagoides pteronyssinus (house dust mite) IgE	Serum	0.15 kIU/L	*(63)*
Fibrinogen	Serum	10 mg/L	*(64)*
Niacinamide	Serum, urine	1 nmol/L	*(65)*
Total IgE	Serum	5 kIU/L	*(66)*
Transferrin	Serum	0.16 mg/L	*(17)*

[a] Ag, antigen.

measure hybridization of nucleotides, particularly single-stranded DNA, has grown dramatically since 1996 (Fig. 2B). Recent work has shown that it is possible to sensitively and specifically detect genetically modified organisms (GMOs) and even single base-pair mismatches from PCR-amplified contaminated foodstuffs and pooled patient sera *(19*, *20*, *48*, *49)*. Specific detection of GMOs was achieved by use of synthetic oligonucleotide probes specific for plasmid sequences that were unique to the relevant modified organism. DNA isolated from certified reference materials and real GMO-contaminated samples were subjected to PCR and then hybridized to either thiolated and biotinylated single-stranded DNA probes immobilized on the surface of an acoustic quartz biosensor *(48)*. The advantages of such an approach compared with electrophoretic post-PCR detection were claimed to be the label-free nature of the measurement, the lack of toxic reagents (i.e., ethidium bromide), and the reusability of the sensor (more than 20 measurements possible per sensor). The same group has also described an acoustic method to determine one of the most frequent mutation characteristics of β-thalassemia in the Mediterranean population: the C-to-T substitution in codon 39 of the β-globin gene *(50)*. The system was able to detect sequences differing in only 1 base by use of a 25-bp probe sequence together with PCR-amplified pooled serum samples containing genotype-specific 771- and 577-bp sequences.

The ability to probe for pathogen nucleic acid, pathogen antigen, and pathogen-specific host antibodies can provide for extra assay redundancy, giving greater confidence in the results. In time, this capacity could enable the development of very robust and precise pathogen detection systems that give information on pathogen copy number, antigen concentration, and immunologic host response.

INSTRUMENT DEVELOPMENT

The breadth of application areas described above is considerable, with numerous published reports describing the detection of nearly all classes of clinically relevant analytes. However, it is surprising that these data have almost exclusively been generated by use of home-built QCM systems, often with insufficient attention to surface chemistry and assay reproducibility. A widely available and robust acoustic detection system that can generate reproducible data for the above classes of analytes could be of great benefit to the life sciences research, clinical diagnostics, environmental sensing, and homeland defense communities. In response to this challenge, we are developing RAP systems that incorporate several key technical advances compared with the prior art. We have produced high-frequency resonators that possess high merit or "Q" factors (a measure of the ability of a piezoelectric device to convert electrical energy into kinetic energy). This increases the detection sensitivity *(23)* and also improves assay reproducibility. These resonators incorporate a parallel reference control, which enables analyte to be passed simultaneously over both the active and control receptors. Real-time subtraction of control data from active data will further improve the robustness of the assay.

There have been major advances in the field of microfluidics that enable sophisticated devices to be developed, tested, and ultimately released to the market over a much shorter time scale than was possible a decade ago. Because quartz is a piezoelectric material, it is highly sensitive to flexural, shear, and pressure changes. These artifacts are undesirable in a system designed to measure a specific response to analyte. To address this potential problem, we have combined a proprietary stress-free mounting system for the quartz crystal with a microfluidic lateral flow device. This ensures that the detector response is sensitive principally to analyte binding. It also enables a relatively small (<10 μL) volume of liquid to be delivered and removed from the resonant sensing area rapidly and efficiently with minimal sample dispersion or sample cross-contamination (Fig. 1).

LINKER CHEMISTRY

The interface between the biosensor surface and the chemical or biological systems to be studied is a vital component of all surface-sensitive sensor systems. Receptors must be attached to some form of solid support while retaining their native conformation and binding activity. This attachment must be stable over the course of a binding assay; in addition, sufficient binding sites must be presented to the solution phase to interact with the analyte. Most importantly, the support must be resistant to nonspecific binding of the sample matrix, which could mask the signal produced by analyte binding. Many receptor-coupling strategies use a chemical linker layer between the sensor base interface (e.g., a gold layer) and the biological component to achieve these ends. The termini of these molecules can be derivatized with molecules that possess suitable chemical reactivities for receptor capture (e.g., epoxy, carboxyl, amino, biotinyl, or nitrilotriacetic acid) *(51–53)*. The receptor typically is immobilized on the surface, and the binding partner (analyte) is allowed to bind to this surface from free solution. However, it is also possible to configure solution competition assays in which the analyte is immobilized on the surface and competes with solution-phase analyte for receptor.

Selection of the correct coupling chemistry requires careful consideration of (*a*) the resulting orientation of receptor, (*b*) its local environment on the surface, (*c*) the stability of the linkage under the conditions used to regenerate the surface, and (*d*) possible effects of the coupling chemistry on components of the binding interaction. In this study, we used a carboxylic acid-terminating linker layer together with carbodiimide-mediated amine coupling (e.g., to surface lysine residues or N-terminal residues on a proteinaceous receptor). If immobilization is performed at low pH, the amine terminus of

the receptor is likely to be more reactive than the γ-amino group of any lysine residues, in which case amine coupling can give rise to more ordered surface orientation. A control receptor (e.g., BSA or nonspecific IgG) was coupled to a control resonator surface, and the active receptor was coupled to an adjacent resonator surface. The reproducibility of the immobilization process is shown in Table 2A for 18 resonators from 4 different batches, with an individual batch CV <10% and a combined CV across all batches <15%. It is also possible to couple sulfhydryl-containing receptors or thiolated oligonucleotide probes by use of chemically selective cross-linking reagents such as 2-(2-pyridinyldithio)ethanamine hydrochloride or 3-(2-pyridinyldithio)propionic acid *N*-hydroxysuccinimide ester to achieve an even higher degree of receptor orientation homology.

RAP ASSAY

After the immobilization of control and active receptors, the resulting "sensor chip" can then be stored for future use or used directly after receptor immobilization. In a typical RAP assay (Fig. 3), at $t = 0$ s, buffer was contacted with the receptor via the microfluidic device. At $t = 60$ s, a solution of analyte (in this case Ms IgG) in the running buffer was passed over the active surface (RaM-Fc) and the control surface (Ms IgG). As the analyte bound to the active receptor, the additional mass and viscoelastic load on the resonator produced a change in the resonance signal (depicted here as a negative change in series resonance).

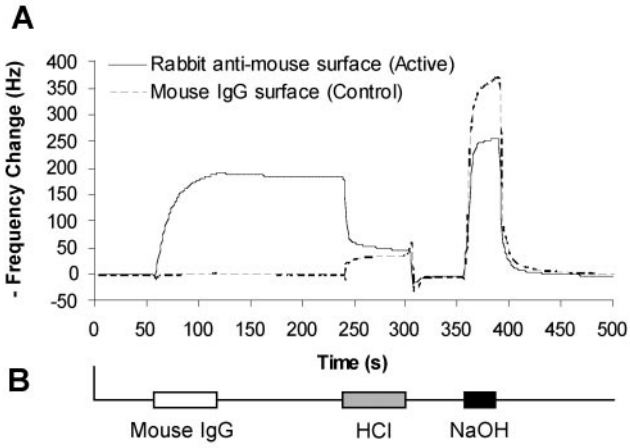

Fig. 3. Example of a typical RAP assay.

(*A*), binding of Ms IgG to RaM-Fc (active) and Ms IgG (control) sensor surfaces. *Solid line* indicates the frequency response generated by binding of Ms IgG to RaM-Fc; *dashed line* indicates the frequency response generated by minimal binding to the control Ms IgG surface. (*B*), schematic representation of sample and regeneration solution injections.

The interassay reproducibility of the binding process,

Table 2. Intra- and interbatch immobilization and binding for interaction of RAM-Fc with Ms IgG.

A. Surface immobilization (frequency changes in Hz) for RaM-Fc and Ms IgG[a]

	RaM-Fc immobilization				Ms IgG immobilization			
Assay	Mean change, Hz	SD, Hz	n	CV, %	Mean change, Hz	SD, Hz	n	CV, %
Intraset variability	499	13	4	2.6	367	29	4	7.8
	503	23	5	4.5	348	11	5	3.2
	446	18	4	4.0	466	31	4	6.6
	495	20	5	4.0	408	20	5	4.8
Interset variability	502	19	18	3.7	395	49	18	12.0

B. Binding responses (frequency changes in Hz) for Ms IgG interacting specifically with RaM-Fc or nonspecifically with Ms IgG[a]

	Ms IgG–RaM-Fc binding				Ms IgG NSB[b]				
Assay	Mean change, Hz	SD, Hz	n	CV, %	Mean change, Hz	SD, Hz	n	S/B ratio	*Z*-factor
Intraset variability	248	14.2	4	5.7	3.5	2.4	4		
	232	2.5	5	1.1	5.0	5.2	3	46	0.90
	235	15.1	6	6.4	2.3	0.8	5	104	0.79
	253	20.1	5	7.9	4.6	1.1	5	55	0.74
Interset variability	239	15.0	20	6.3	3.9	2.8	18	61.48	0.77

C. Repeat of the Ms IgG binding assay on the same sensors[c]

	Ms IgG–RaM-Fc binding				Ms IgG NSB				
Assay	Mean change, Hz	SD, Hz	n	CV, %	Mean change, Hz	SD, Hz	n	S/B ratio	*Z*-factor
Intraset variability	233	11.9	4	5.1	5.5	1.3	4	42	0.83
	226	3.7	5	1.6	4.0	4.4	3	57	0.89
	221	13.9	6	6.3	2.5	1.0	5	88	0.79
	235	21.4	5	9.1	5.0	2.0	5	47	0.69
Interset variability	228	14.4	20	6.3	4.7	2.4	18	49	0.77

[a] Four sensor batches were tested on separate occasions (intraset variability). Data for all 4 batches have also been combined to summarize variability between batches (interset variability).

[b] NSB, nonspecific binding; S/B, signal-to-background.

[c] Binding responses differ from results in Table 2B by less than 10%.

both for the specific binding of mouse IgG to rabbit RaM-Fc and for nonspecific binding of Ms IgG to Ms IgG is summarized in Table 2B, for 18–20 sensors from 4 different batches, with the binding process repeated twice (n = 1 and 2) on each sensor. For this assay, the signal-to-background binding ratios on sensors within the same batch and across all 4 batches were all >40:1, with the CVs all <10%. In addition, the *Z*-factor values for all batches were >0.5, and in all but one case were >0.7, indicating that the specific binding response is very robust and reproducible. Furthermore, repetition of the same binding assay on the same sensor (Table 2C) showed that the intraassay variability was consistently <10%.

Analysis of the association phase of the binding curve can give the observed association rate (k_{obs}). If the concentration of the analyte is known, then the association rate constant of the interaction (k_{ass}) can be determined. At t = 240 s, the Ms IgG solution was replaced by buffer, and the receptor–analyte complex was allowed to dissociate. Analysis of these data can give the dissociation rate constant (k_{diss}) for the interaction. Many complexes in biology have considerable half-lives; thus, a pulse of a regeneration solution (in this case an acid wash followed by a basic wash) was used at t = 240 s and 360 s to disrupt binding and regenerate the free receptor. The entire binding cycle can be repeated many times at various analyte concentrations to generate a robust data set for global fitting to an appropriate binding algorithm. The affinity of the interaction can be calculated from the ratio of the rate constants ($K_D = 1/K_A = k_{diss}/k_{ass}$) or by a linear or nonlinear fitting of the response at equilibrium vs various concentration of analyte.

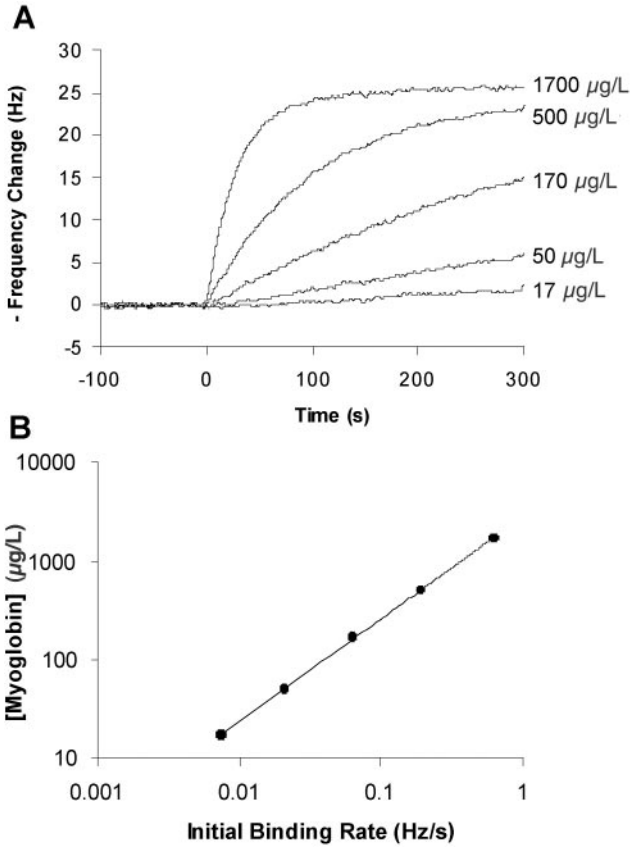

Fig. 4. Myoglobin RAP assay.

(*A*), binding of recombinant human myoglobin to mouse anti-myoglobin antibody, previously captured on a RaM-Fc surface. Binding curves for 5 different myoglobin concentrations (1700, 500, 170, 50, and 17 μg/L; equivalent to 100, 30, 10, 3, and 1 nmol/L) are shown overlaid and synchronized to the start of each myoglobin injection. Correction for signal drift attributable to the off-rate of the captured anti-myoglobin antibody was performed by subtraction of the response from injection of buffer only. (*B*), myoglobin concentration–response calibration curve, generated by plotting the initial binding rate for the set of standard concentrations. Estimates of myoglobin concentration in unknown samples were calculated by linear interpolation from the calibration curve with an accuracy of 0.5%–15% over the concentration range tested.

MYOGLOBIN

Myoglobin is a 17-kDa cytoplasmic protein, found in muscle cells, that binds and stores oxygen. Myoglobin concentrations in blood usually are very low (<100 μg/L). After muscle damage (e.g., cardiac ischemia), however, myoglobin is released into the blood, and concentrations can increase to >1000 μg/L immediately after a myocardial infarction and can remain high (~ 500 μg/L) for some time afterward. Detection of myoglobin in blood is therefore a good diagnostic indicator of preceding and ongoing cardiac disease and damage *(54)*. We used a mouse anti-myoglobin antibody, previously captured on a RaM-Fc surface to measure binding of various concentrations of human recombinant myoglobin in real time (Fig. 4A). Different concentrations of myoglobin in the sample would give different responses at equilibrium, which would enable generation of a calibration curve for analyte concentration. However, as can be seen in Fig. 4A, at lower myoglobin concentrations considerable contact time would be required to reach equilibrium. In addition, in a "real-world" diagnostic application, the sensor is likely to be used only once and receptor activity may vary after shipping and storage, which would lead to variable equilibrium binding characteristics. Hence, analyte concentration can be more accurately and rapidly determined by analyzing the rate of binding of myoglobin to the antibody and comparing the measured observed association rate with a data set calibrated to analyte concentration (Fig. 4B). This enabled the myoglobin concentration in the sample to be determined in less than 6 min.

IL-1β

Members of the IL-1 family have clear therapeutic and diagnostic potential: the IL-1 agonists IL-1a and IL-1β are induced by central nervous system injury, whereas peripheral or central administration of the IL-1 antagonist IL-1ra reduces the extent of damage by more than 50%. The mechanism of action of these cytokines is the subject of intense research *(55)*. IL-1β is a 17.3-kDa protein found in serum, mucosa, and pleural effusions of different etiologies. It has been suggested as a diagnostic marker in the differential diagnosis of several pleural diseases *(56)* and has also been found in consistently increased concen-

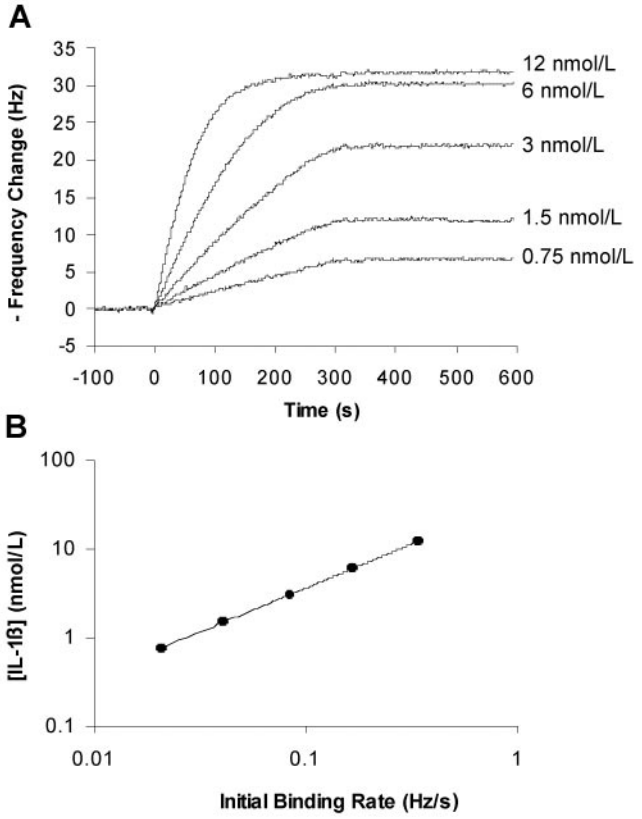

Fig. 5. IL-1β RAP assay.

(*A*), binding of human IL-1β to mouse anti-IL-1β antibody previously captured on a RaM-Fc surface. Binding curves for 5 different IL-1β concentrations are shown overlaid, synchronized to the start of each IL-1β injection. Data have been normalized by subtraction of the response to injection of buffer alone, to correct for the off-rate of the captured anti-IL-1β antibody. (*B*), IL-1β concentration–response calibration curve. The initial binding rate for each IL-1β concentration was calculated as for the myoglobin concentration–response calibration curve (Fig. 4).

trations in normal-appearing mucosa from patients with Crohn disease, potentially providing evidence for a sustained immune stimulation in Crohn disease in the absence of patent inflammation *(57)*. We used a mouse anti-IL-1β antibody, previously captured on a RaM-Fc surface, to bind various concentrations of human IL-1β (Fig. 5A). As in the case for myoglobin, analyte concentration was more accurately and rapidly determined by analyzing the rate of binding of IL-1β to the antibody and comparing the measured observed association rate with a data set calibrated to analyte concentration (Fig. 5B). This also enabled the concentration of IL-1β in the sample to be determined in less than 6 min.

GLUCOSE DEHYDROGENASE

Glucose dehydrogenase (GDH) is a key initial enzyme in the energy production process that uses nucleotide cofactors to "activate" monosaccharide sugars as a prelude to their subsequent breakdown into pyruvate to enter the Krebs cycle. $NADP^+$ (765 Da) is the preferred cofactor, and NAD^+ (663 Da) will act as a lower activity cofactor, but FAD (830 Da) will not bind or act as cofactor. Preferred monosaccharide substrates for the enzyme are glucose and galactose (180 Da). Other monosaccharides, e.g., fructose (180 Da), and disaccharides, e.g., maltose and sucrose (342 Da), cannot act as substrates.

GDH was coupled to a carboxylic acid–terminating linker layer by standard carbodiimide amine coupling as described earlier. BSA was coupled in a similar manner to a second sensor surface to be used as a passive control. $NADP^+$, NAD^+, and FAD were then independently serially diluted and injected across the GDH active and BSA control surfaces for 1 min. The complexes were then allowed to dissociate for 1 min until prebinding baseline

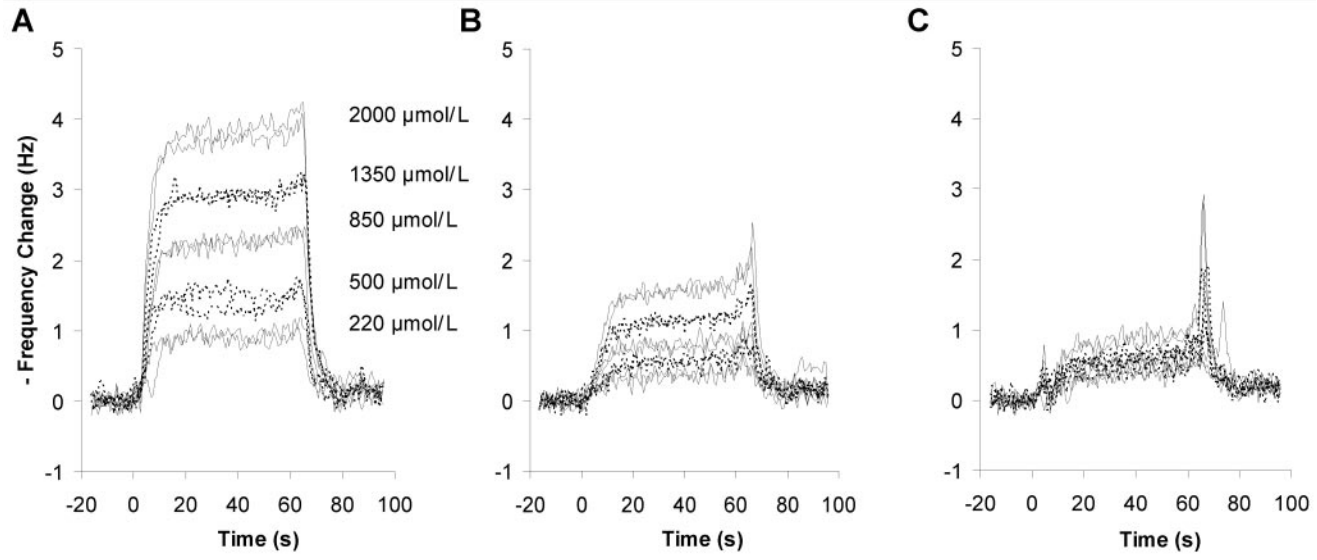

Fig. 6. Binding of preferred substrate, poor substrate, and nonpreferred substrate adenine nucleotide cofactors to the metabolic enzyme GDH.

(*A*), NADP (765 Da; preferred substrate) binding shows a clear equilibrium concentration–response relationship. (*B*), NAD (663 Da; metabolite) shows a lower equilibrium binding and compressed concentration–response relationship. (*C*), FAD (830 Da; nonpreferred substrate) shows very low equilibrium binding.

values were attained (Fig. 6). From simple visual inspection of the magnitude of the binding responses of the different cofactors, a rapid estimate of ranking affinity can be made: $NADP^+ > NAD^+ > FAD$. The equilibrium binding constant, K_D, for $NADP^+$ binding to GDH was calculated from analysis of equilibrium binding values resulting from injection of 3-fold dilutions of $NADP^+$. The mean response during the "plateau" phase of binding (Fig. 7A) was plotted against $NADP^+$ concentration, and these data were fitted to a sigmoidal single-site binding model (Fig. 7B) to give a K_D of 2.8 mmol/L. This demonstrates that RAP can be used for accurate determination of cofactor affinities for an enzyme in real time in <20 min.

CONCLUSION

Rapid identification of predictive disease markers, pathogens, and toxins that cause infections or have other deleterious effects on human health brings many benefits, including rapid institution of specific therapy and appropriate infection control measures *(58)*. Application of rapid methods in routine practice has, unfortunately, lagged behind their adoption in other areas of medicine, in part because of the need to grow organisms and isolate them in pure culture before they can be identified. Although PCR methods can provide valuable early results in some situations, local facilities are not available to most laboratories, and specimens are often transported to reference laboratories for such tests. Current diagnostic techniques suffer from several limitations, including insufficient sensitivity (low-level infections may not be detected unless amplification techniques are used, which imposes severe restrictions because of the need for expensive laboratory equipment and facilities) and speed (current assays generally rely on optical techniques, which require separation of plasma from erythrocytes before measurement, which in turn increases the time to result and can be difficult to do in nonlaboratory environments). In recognition of these limitations, Akubio is developing a proprietary acoustic detection technology, Resonant Acoustic Profiling (RAP), that promises to provide increases in speed, throughput, and sensitivity over established methodologies. Early data from this system suggest that the technology could potentially form a core detection module for new clinical tests. The system can detect most classes of clinically relevant analytes in real time without enzymatic, fluorescent, isotopic, or chemiluminescent labels. However, much work is still required to improve sensitivity (limits of detection) and specificity (effects of interferents). Initial applications of the technology will most likely be in the areas of reagent validation and assay development. In those areas, the real-time, label-free nature of the assay can give rapid, accurate information regarding molecular interaction affinities, specificities, and kinetics. The system is entirely electronic and has modest requirements for power and data processing compared with analogous optical systems. Hence, assays in the future could potentially be carried out both in the laboratory and at the point of use, e.g., in a patient's home, at a hospital bedside, or in the field.

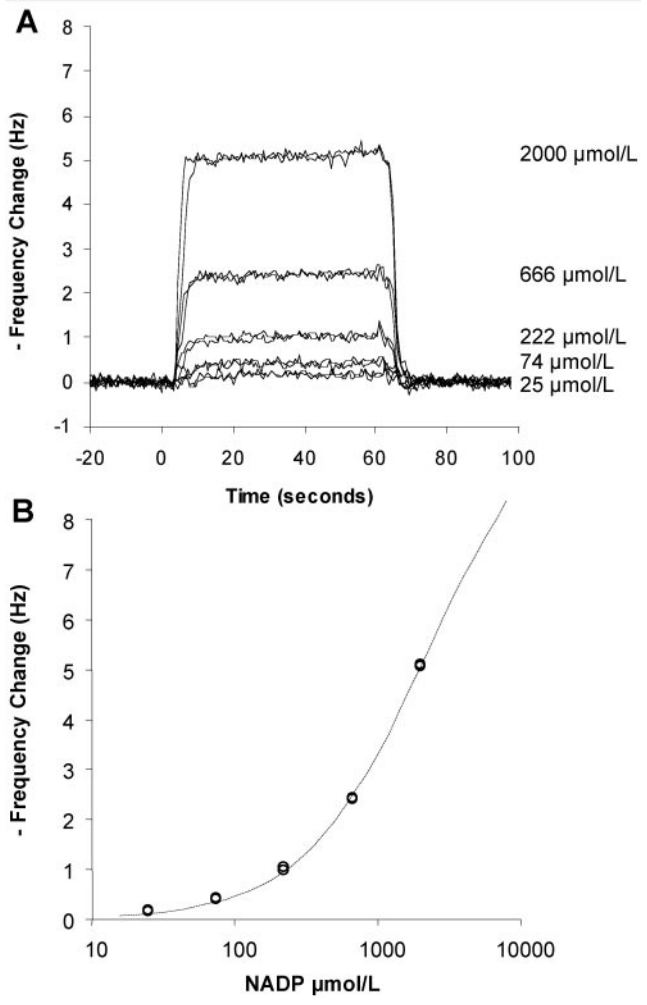

Fig. 7. Binding of $NADP^+$ to GDH.

(*A*), equilibrium binding of 5 different concentrations of $NADP^+$ to immobilized GDH. (*B*), $NADP^+$ sigmoidal concentration–response curve generated from the equilibrium binding values. These were calculated as the mean response over a 10-s interval during the plateau phase for each $NADP^+$ concentration response. K_D calculated from the binding curve is 2.8 mmol/L.

References

1. Ward MD, Buttry DA. In situ interfacial mass detection with piezoelectric transducers. Science 1990;249:1000–7.
2. Curie J, Curie P. Piezoelectric and allied phenomena in Rochelle salt. Comput Rend Acad Sci Paris 1880;91:294–7.
3. Sauerbrey G. Verwendung von Schwingquarzen zur Wagung dunner Schichten und zur Microwagang. Z Phys 1959;155:206–12.
4. Nomura T, Okuhara M. Frequency-shifts of piezoelectric quartz crystals immersed in organic liquids. Anal Chim Acta 1982;142:281–4.
5. Auge J, Hauptmann P, Hartmann J, Rosler S, Lucklum R. New design for QCM sensors in liquids. Sens Actuators B Chem 1995;24:43–8.
6. Pavey KD, Olliff CJ, Paul F. Quartz crystal resonant sensor (QCRS) model for label-free, small molecules—receptor studies. Analyst 2001;126:1711–5.
7. Pope LP, Allen S, Roberts CJ, Tendler SJB, Williams PM. Probing

DNA duplex formation and DNA-drug interactions by the quartz crystal microbalance technique. Langmuir 2001;17:8300–4.

8. Pavey KD, Miah M, Fucassi F, Paul F, Cragg PJ. Vitamin C induced decomposition of lipid hydroperoxides: direct evidence of genotoxin-DNA binding detected by QCRS. Chem Commun 2001;18: 1886–7.
9. Furtado LM, Su HB, Thompson M, Mack DP, Hayward GL. Interactions of HIV-1 TAR RNA with Tat-derived peptides discriminated by on-line acoustic wave detector. Anal Chem 1999;71:1167–75.
10. Thompson M, Su HB. Realtime detection of HIV-1 TAR RNA/Tat peptide interactions by acoustic wave biosensor. Abstr Pap Am Chem Soc 1996;212:80-IEC.
11. Thompson M, Su HB, McGovern M, Kwong K, Mack D. Comparison of detection of RNA-peptide interactions by surface plasmon resonance and acoustic wave transmission. Abstr Pap Am Chem Soc 1997;213:213-ANYL.
12. Aizawa H, Kurosawa S, Ogawa K, Yoshimoto M, Miyake J, Tanaka H. Conventional diagnosis of C-reactive protein in serum using latex piezoelectric immunoassay. Sens Actuators B Chem 2001; 76:173–6.
13. BenDov I, Willner I, Zisman E. Piezoelectric immunosensors for urine specimens of *Chlamydia trachomatis* employing quartz crystal microbalance microgravimetric analyses. Anal Chem 1997;69:3506–12.
14. Ghourchian HO, Kamo N. Latex piezoelectric immunoassay—effect of Interfacial properties. Anal Chim Acta 1995;300:99–105.
15. Kurosawa S, Aizawa H, Yoshimoto M. Latex piezoelectric immunoassay: analysis of C-reactive protein in human serum. IEEE Trans Ultrason Ferroelectr Freq Control 2000;47:1256–8.
16. Percival CJ, Stanley S, Braithwaite A, Newton MI, McHale G. Molecular imprinted polymer coated QCM for the detection of nandrolone. Analyst 2002;127:1024–6.
17. Wu ZY, Shen GL, Xie LJ, Yu RQ. A PEG piezoelectric immunoassay for the determination of transferrin in human serum. Sens Actuators B Chem 2000;71:99–105.
18. Suleiman AA, Guilbault GG. Piezoelectric (Pz) immunosensors and their applications. Anal Lett 1991;24:1283–92.
19. Hook F, Ray A, Norden B, Kasemo B. Characterization of PNA and DNA immobilization and subsequent hybridization with DNA using acoustic-shear-wave attenuation measurements. Langmuir 2001; 17:8305–12.
20. Caruso F, Furlong DN, Niikura K, Okahata Y. In-situ measurement of DNA immobilization and hybridization using a 27 MHz quartz crystal microbalance. Colloids Surf B Biointerfaces 1998;10: 199–204.
21. Hengerer A, Kosslinger C, Decker J, Hauck S, Queitsch I, Wolf H, et al. Determination of phage antibody affinities to antigen by a microbalance sensor system. Biotechniques 1999;26:956–60, 962, 964.
22. Hengerer A, Decker J, Prohaska E, Hauck S, Kosslinger C, Wolf H. Quartz crystal microbalance (QCM) as a device for the screening of phage libraries. Biosens Bioelectron 1999;14:139–44.
23. Uttenthaler E, Schraml M, Mandel J, Drost S. Ultrasensitive quartz crystal microbalance sensors for detection of M13-phages in liquids. Biosens Bioelectron 2001;16:735–43.
24. Zhou XD, Liu LJ, Hu M, Wang LL, Hu JM. Detection of hepatitis B virus by piezoelectric biosensor. J Pharm Biomed Anal 2002;27: 341–5.
25. Susmel S, O'Sullivan CK, Guilbault GG. Human cytomegalovirus detection by a quartz crystal microbalance immunosensor. Enzyme Microbiol Technol 2000;27:639–45.
26. Sato T, Serizawa T, Okahata Y. Binding of influenza A virus to monosialoganglioside (GM3) reconstituted in glucosylceramide and sphingomyelin membranes. Biochim Biophys Acta 1996; 1285:14–20.
27. Fung YS, Wong YY. Self-assembled monolayers as the coating in a quartz piezoelectric crystal immunosensor to detect salmonella in aqueous solution. Anal Chem 2001;73:5302–9.
28. Otto K, Elwing H, Hermansson M. Effect of ionic strength on initial interactions of *Escherichia coli* with surfaces, studied on-line by a novel quartz crystal microbalance technique. J Bacteriol 1999; 181:5210–8.
29. Spangler BD, Wilkinson EA. Evaluation of small-scale quartz-crystal microbalance and surface-plasmon-resonance biosensors for detection of bacterial pathogens. Abstr Pap Am Chem Soc 2000;219:U115.
30. Wong YY, Ng SP, Ng MH, Si SH, Yao SZ, Fung YS. Immunosensor for the differentiation and detection of Salmonella species based on a quartz crystal microbalance. Biosens Bioelectron 2002;17: 676–84.
31. Pavey KD, Ali Z, Olliff CJ, Paul F. Application of the quartz crystal microbalance to the monitoring of *Staphylococcus epidermidis* antigen-antibody agglutination. J Pharm Biomed Anal 1999;20: 241–5.
32. Pavey KD, Barnes LM, Hanlon GW, Olliff CJ, Ali Z, Paul F. A rapid, non-destructive method for the determination of Staphylococcus epidermidis adhesion to surfaces using quartz crystal resonant sensor technology. Lett Appl Microbiol 2001;33:344–8.
33. Richert L, Lavalle P, Vautier D, Senger B, Stoltz JF, Schaaf P, et al. Cell interactions with polyelectrolyte multilayer films. Biomacromolecules 2002;3:1170–8.
34. Rodahl M, Hook F, Fredriksson C, Keller CA, Krozer A, Brzezinski P, et al. Simultaneous frequency and dissipation factor QCM measurements of biomolecular adsorption and cell adhesion. Faraday Discuss 1997:229–46.
35. Fredriksson C, Kihlman S, Rodahl M, Kasemo B. The piezoelectric quartz crystal mass and dissipation sensor: a means of studying cell adhesion. Langmuir 1998;14:248–51.
36. Shinohara H. Real time monitoring of growth and adhesion of cultured mammalian cells with quartz crystal microbalance systems and its applications. Electrochemistry 1999;67:280–4.
37. Ebato H, Okahata Y, Matsuda T. Detection of cell-adhesion behaviors by using a quartz-crystal microbalance. Kobunshi Ronbunshu 1993;50:463–9.
38. Gryte DM, Ward MD, Hu WS. Real-time measurement of anchorage-dependent cell-adhesion using a quartz crystal microbalance. Biotechnol Progr 1993;9:105–8.
39. Ebersole RC, Foss RP, Ward MD. Piezoelectric cell-growth sensor. Biotechnology 1991;9:450–4.
40. Braunhut SJ, Marx KA, Zhou T, Warren MC, Schulze HM. Endothelial cell (EC) adhesion and spreading studied with the quartz crystal microbalance (QCM). Mol Biol Cell 1999;10:64a-a.
41. Wegener J, Seebach J, Janshoff A, Galla HJ. Analysis of the composite response of shear wave resonators to the attachment of mammalian cells. Biophys J 2000;78:2821–33.
42. Cooper MA. Optical biosensors in drug discovery. Nat Rev Drug Discov 2002;1:515–28.
43. Thompson M, Hayward GL. Mass response of the thickness-shear mode acoustic wave sensor in liquids as a central misleading dogma. Proceedings of the 1997 IEEE International Frequency Control Symposium, May 28–30, 1997, Orlando, FL: 114–9.
44. Janshoff A, Galla HJ, Steinem C. Piezoelectric mass-sensing devices as biosensors—an alternative to optical biosensors? Angew Chem Int Ed Engl 2000;39:4004–32.
45. Schroder J, Borngraber R, Eichelbaum F, Hauptmann P. Advanced interface electronics and methods for QCM. Sens Actuators A Phys 2002;97-8:543–7.
46. Borngraber R, Schroder J, Lucklum R, Hauptmann P. Is an

oscillator-based measurement adequate in a liquid environment? IEEE Trans Ultrason Ferroelectr Freq Control 2002;49:1254–9.
47. Lucklum R, Hauptmann P. Transduction mechanism of acoustic-wave based chemical and biochemical sensors. Meas Sci Technol 2003;14:1854–64.
48. Mannelli I, Minunni M, Tombelli S, Mascini M. Quartz crystal microbalance (QCM) affinity biosensor for genetically modified organisms (GMOs) detection. Biosens Bioelectron 2003;18:129–40.
49. Minunni M, Tombelli S, Mariotti E, Mascini M. Biosensors as new analytical tool for detection of genetically modified organisms (GMOs). Fresenius J Anal Chem 2001;369:589–93.
50. Minunni M, Tombelli S, Scielzi R, Mannelli I, Mascini M, Gaudiano C. Detection of β-thalassemia by a DNA piezoelectric biosensor coupled with polymerase chain reaction. Anal Chim Acta 2003; 481:55–64.
51. Lahiri J, Isaacs L, Tien J, Whitesides GM. A strategy for the generation of surfaces presenting ligands for studies of binding based on as active ester as a common reactive intermediate: a SPR study. Anal Chem 1999;71:777–90.
52. Sigal GB, Bamdad C, Barberis A, Strominger J, Whitesides GM. A self-assembled monolayer for the binding and study of histidine tagged proteins by surface plasmon resonance. Anal Chem 1996; 68:490–7.
53. Ernst OP, Bieri C, Vogel H, Hofmann KP. Intrinsic biophysical monitors of transducin activation: UV-visible spectroscopy, light scattering and evanescent field techniques. Methods Enzymol 2000;315:471–89.
54. Casey PE. Markers of myocardial injury and dysfunction. AACN Clin Issues 2004;15:547–57.
55. Gibson RM, Rothwell NJ, Le Feuvre RA. CNS injury: the role of the cytokine IL-1. Vet J 2004;168:230–7.
56. Silva-Mejias C, Gamboa-Antinolo F, Lopez-Cortes LF, Cruz-Ruiz M, Pachon J. Interleukin-1β in pleural fluids of different etiologies. Its role as inflammatory mediator in emphysema. Chest 1995;108: 942–5.
57. Reimund JM, Wittersheim C, Dumont S, Muller CD, Kenney JS, Baumann R, et al. Increased production of tumour necrosis factor-α interleukin-1 β, and interleukin-6 by morphologically normal intestinal biopsies from patients with Crohn's disease. Gut 1996;39:684–9.
58. Henderson DA. The looming threat of bioterrorism. Science 1999; 283:1279–82.
59. Uttenthaler E, Kosslinger C, Drost S. Characterization of immobilization methods for African swine fever virus protein and antibodies with a piezoelectric immunosensor. Biosens Bioelectron 1998;13:1279–86.
60. Wang H, Lei CX, Li JS, Wu ZY, Shen GL, Yu RQ. A piezoelectric immunoagglutination assay for *Toxoplasma gondii* antibodies using gold nanoparticles. Biosens Bioelectron 2004;19:701–9.
61. Aizawa H, Kurosawa S, Tanaka M, Wakida S, Talib ZA, Park JW, et al. Conventional diagnosis of *Treponema pallidum* in serum using latex piezoelectric immunoassay. Mater Sci Eng C Bio S 2001; 17:127–32.
62. Hu JM, Pei RJ, Hu Y, Zeng YE. Detection of complement C4 with a piezoelectric immunosensor. Chin J Chem 1998;16:219–25.
63. Su XD, Chew FT, Li SFY. Piezoelectric quartz crystal based label-free analysis for allergy disease. Biosens Bioelectron 2000; 15:629–39.
64. Aizawa H, Kurosawa S, Tozuka M, Park JW, Kobayashi K, Tanakac H. Conventional detection method of fibrinogen and fibrin degradation products using latex piezoelectric immunoassay. Biosens Bioelectron 2003;18:765–71.
65. Long Y, Li W, Nie L, Yao S. Ion-selective piezoelectric sensor for niacinamide assay in serum and urine. J Pharm Biomed Anal 2001;24:361–9.
66. Su XD, Chew FT, Li SFY. Self-assembled monolayer-based piezoelectric crystal immunosensor for the quantification of total human immunoglobulin E. Anal Biochem 1999;273:66–72.